Two-photon absorption laser induced fluorescence (TALIF) detection of atomic iodine in low-temperature plasmas and a revision of the energy levels of I I

Benjamin Esteves, Christophe Blondel, Pascal Chabert, Cyril Drag

Journal of Physics B: Atomic, Molecular and Optical Physics

Two-photon absorption laser induced fluorescence (TALIF) detection of atomic iodine in low-temperature plasmas and a revision of the energy levels of I I

To cite this article before publication: Benjamin Esteves *et al* 2023 *J. Phys. B: At. Mol. Opt. Phys.* in press https://doi.org/10.1088/1361-6455/acb7b6

Two-photon absorption laser induced fluorescence (TALIF) detection of atomic iodine in low-temperature plasmas and a revision of the energy levels of I I

Benjamin Esteves, Christophe Blondel, Pascal Chabert, Cyril Drag

Laboratoire de Physique des plasmas, Centre national de la recherche scientifique, Sorbonne Université, Université Paris-Saclay, Observatoire de Paris, École polytechnique, Institut polytechnique de Paris, route de Saclay, F-91128 Palaiseau cedex, France

E-mail: christophe.blondel@lpp.polytechnique.fr

October 2022

Abstract. In order to perfect the use of iodine, instead of xenon, in plasma thrusters, an experiment has been set up to investigate the feasibility of two-photon absorption laser induced fluorescence (TALIF) diagnostics in iodine plasmas. Levels $(^3P_2)6p\,^2[1]^o_{3/2}$ and $(^3P_2)6p\,^2[3]^o_{7/2}$ of atomic iodine were found qualified for that purpose, with a radiative lifetime of the former found equal to 35.5(9) ns, which appears consistent with the 32.5(1.2) ns predicted by the most recent calculations.

Doppler-free two-photon spectroscopy has confirmed that the relative intensities of the hyperfine components follow well-known general formulas, which makes it possible to disentangle the hyperfine structure of ^{127}I from Doppler broadening. Accurate temperature measurements are shown to be possible, even though the relatively heavy mass of the iodine atom does not make it the most favorable gauge for measurements based on Doppler effect. Using an injection seeded pulsed laser as the primary laser source, the frequency-tripling of which has provided the ca 300 nm radiation used for excitation, absolute energy measurements of the two-photon excited levels revealed that all upper energy levels of I I have to be revised down, by $-0.169(11)\mathrm{cm}^{-1}$, which pulls every energy level off its presently tabulated value by more than thirty times the currently admitted uncertainty bar.

1. Introduction

Plasma propulsion engines are based on obtaining force through an accelerated quasi-neutral plasma. The idea is one century old (Brewer et al. 1961), with implementations beginning in the 1960s and ongoing investigations (Mazouffre 2016). Standard plasma thrusters have in common that they accelerate positive xenon ions (Xe^+) to produce thrust. Xenon is rare and expensive and an alternative, which has been studied for

about ten years all over the world (Esteves et al. (2022) and references therein), is to use iodine as a propellant. Iodine is available in abundance on earth and not very expensive. With a $Z = 53$ charge number next lower to the one of xenon and naturally present in molecular form, iodine can advantageously replace xenon because of the low dissociation energy of I_2 and low ionization energies of both I and I_2. Iodine can be easily stored in a solid form and only requires light heating for gas production. The in-flight demonstration of a satellite using an iodine plasma was reported recently (Rafalskyi et al. 2021) and the Busek© company already markets Hall-effect thrusters fueled by iodine.

However, even though many investigations have been carried out on iodine plasmas, they have been made mainly outside the context of propulsion (Stewart et al. 1964, Woolsey et al. 1973, Liebl & Harrison 1976). In a molecular plasma, the electrical energy supplied to the electrons is used to ionize the molecules, but this energy is also dissipated in electronic, vibrational and rotational heating of the molecules. In addition, the transport phenomena are also different in molecular gases, and the relaxation length of the electron energy is expected to be shorter in iodine than in noble gases (Esteves et al. 2022). A significant fraction of negative ions is also expected given the very high effective cross section for dissociative attachment (Ambalampitiya et al. 2021).

To guide the theoretical calculations concerning the operation of thrusters (Grondein et al. 2016, Levko & Raja 2021), especially at low pressure, the literature lacks basic data describing the chemical reactions of various species, although there is a renewed interest in new calculations, such as electron impact collisions cross-sections on I and I_2 (Ambalampitiya et al. 2021) or line strengths and atomic probabilities for some transitions of neutral iodine (Filin et al. 2020). Electrical or optical diagnostics are also rare. A LIF scheme has been studied on I^+ (Steinberger & Scime 2018) and measurements of the ratio between I^+ and I_2^+ were performed using a mass spectrometer, at the output of a radio frequency ion thruster (Dietz et al. 2019). The behavior of electrons was studied by Langmuir probe and laser photodetachment was used to probe negative ions in a low-pressure inductively-coupled plasma chamber used as the ionization stage of a gridded ion-engine (Esteves et al. 2022).

The methods we report here deal with measurements of the temperature of the I atoms and of the relative density of the ground state, by two-photon absorption laser induced fluorescence (TALIF). For those purposes, we use a test plasma, in an iodine cell coupled to an RF generator. The cell pressure is higher than the one generally used in thrusters (the pressure without plasma has been varied from 1.5 Pa to 30 Pa), but already very low compared to more common cold plasmas. The TALIF method is widely used with other atomic or molecular plasmas (Engeln et al. 2020, Gazeli et al. 2021) for density measurements, and also for temperature measurements when the spectral width of the laser is sufficiently narrow compared to Doppler broadening (Booth et al. 2015). This technique has never been applied to iodine plasmas. TALIF has been used to determine the relative populations of I ($^2P^o_{3/2}$) and I ($^2P^o_{1/2}$) atoms following

photodissociation (Brewer et al. 1983, Tiee et al. 1983, Godwin et al. 1987, Tonokura et al. 1993) and to document the absence of I ($^2P^o_{1/2}$) as a product of the reactions of F atoms with HI, I_2, and ICN (Das et al. 1984), even though I ($^2P^o_{1/2}$) was later detected as a scarce product of the F+I_2 reaction (Brunet et al. 1985) through its 1315 nm fluorescence (cf. figure 2). There is, however, no contra-indication to extending the TALIF technique to iodine plasmas. Use of narrowband lasers should even make it possible to monitor not only atomic iodine densities, but also atomic temperatures, the large mass of atomic iodine nothwithstanding. Demonstration of those possibilities has been the aim of the present study.

2. Experimental setup

2.1. The discharge cell

Iodine plasmas are studied using an iodine cell coupled to an RF generator. The quartz cell, without optical coatings, is sealed under vacuum and contains some iodine crystals (shown in operation in figure 1). It is a 25 cm long cylinder with an internal diameter of 3 cm. A 12 cm long and around 1 cm of external diameter "cold finger" is attached to the main cylinder as a reservoir of solid iodine. Temperature regulation of the finger, as long as it remains below room temperature, makes it possible to set the pressure inside the main cylinder. For that purpose, the finger is immersed in a 200 ml beaker, which is temperature-regulated by a ministat 230 controller from Huber, with heat transfer improved by a copper coil. The cooling liquid is a mixture of alcohol and water, which makes it possible to regulate the temperature of the cold point from -10°C to 20°C. Without plasma, pressure as a function of temperature is described in the literature by two empirical formulas that lead to similar values (Kono & Hattori 1979, Tellinghuisen 2011), with a difference that does not exceed 0.1 to 0.8 Pa over the studied temperature range. A thermometer is used to monitor the temperature within the cold beaker and the pressure was varied from 1.5 to 30 Pa.

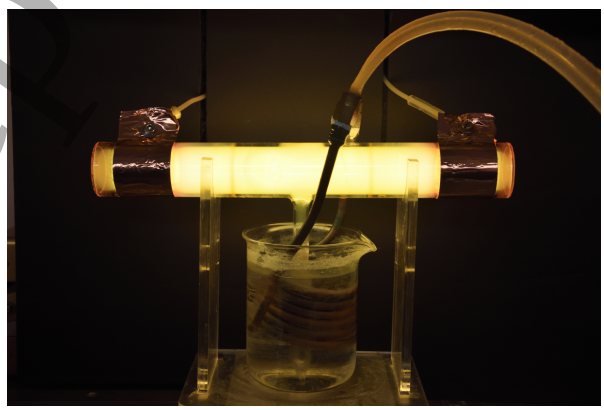

Figure 1. The 25 cm long and 3 cm in-internal-diameter iodine cell. In this example, the "cold finger" temperature is set at 2°C and the cell is excited with an input RF power of 20 W.

Two 35 mm wide copper tape electrodes are placed on the outer surface of the cell and spaced 15 cm apart. These electrodes are connected through an impedance matching circuit to a 13.56 MHz RF generator from Sairem. The input and reflected powers are measured by a Vigilant Monitor probe from Solayl. The RF power is the difference between the incident and the reflected powers. Two problems can appear with this cell used to produce a plasma: (i) The power must be limited so that a plasma is not present in the "cold finger". In such conditions, the temperature increases and it is no longer possible to consider the discharge perfectly cylindrical. (ii) We also observed that a high plasma power could make the cell opaque, certainly due to etching of the internal surfaces. The optical transmission can be partially restored by heating the cell with a heat gun. However, we have never recovered the initial optical quality, which deteriorates with the operating time when a plasma is on.

As a whole, the plasma tube appears similar to the classical glow discharge tubes used historically. The electron temperature T_e lies typically between 20000 and 50000 K, depending on the neutral gas pressure (T_e decreases with pressure). Using an RF excitation instead of the more usual DC one prevents metallic contamination from the electrodes and also makes it possible to reach somewhat higher electron densities. In our experiments the electron density typically varied from 10^{15} to $10^{17}\,\mathrm{m}^{-3}$, from the lowest to the highest power used. Because iodine is an electronegative gas, there can also be a significant fraction of negative ions. This leads to Debye lengths ranging from tens of microns up to a fraction of a millimetre, depending on the conditions.

2.2. TALIF optical setup

The TALIF method consists in recording the fluorescence signal that follows the resonant absorption of two photons of UV light. The first levels accessible by a two-photon odd-parity preserving transition, starting from the $5s^25p^5\,{}^2P^o_{3/2}$ ground level of I, are those of the $5s^25p^4(^3P_2)6p^o$ electron configuration, located around $65000\,\mathrm{cm}^{-1}$. Among these, we mainly applied excitation towards the $(^3P_2)6p\,{}^2[1]^o_{3/2}$ level, with detection of the fluorescence at 804 nm. Occasionally, we also excited the $(^3P_2)6p\,{}^2[3]^o_{7/2}$ level, which fluoresces only at 905 nm (cf. figure 2).

2.2.1. Lasers. The experimental scheme is shown in figure 3. To produce the radiation around 300 nm, a commercial singlemode continuous titanium:sapphire (Ti:Sa) laser (Coherent MBR 110 pumped by a 10 W Verdi Nd:YAG laser) was used as the master laser to injection-seed a home-built nanosecond pulsed Ti:Sa (slave) laser (Lottigier et al. 2019). The frequency of the seed laser (operating around 900 nm) was monitored by a wave-meter (Ångstrom WSU from High Finesse, with a measurement resolution of 5 MHz FWHM and a precision of 30 MHz) calibrated daily with a ^{133}Cs saturated-absorption stabilized diode laser. Reliability of the calibration process could be checked measuring the wavenumber of the other Cs D line, as explained in more details in section 3.2. The slave laser comprised a Ti:Sa crystal pumped at 532 nm by a 20 Hz

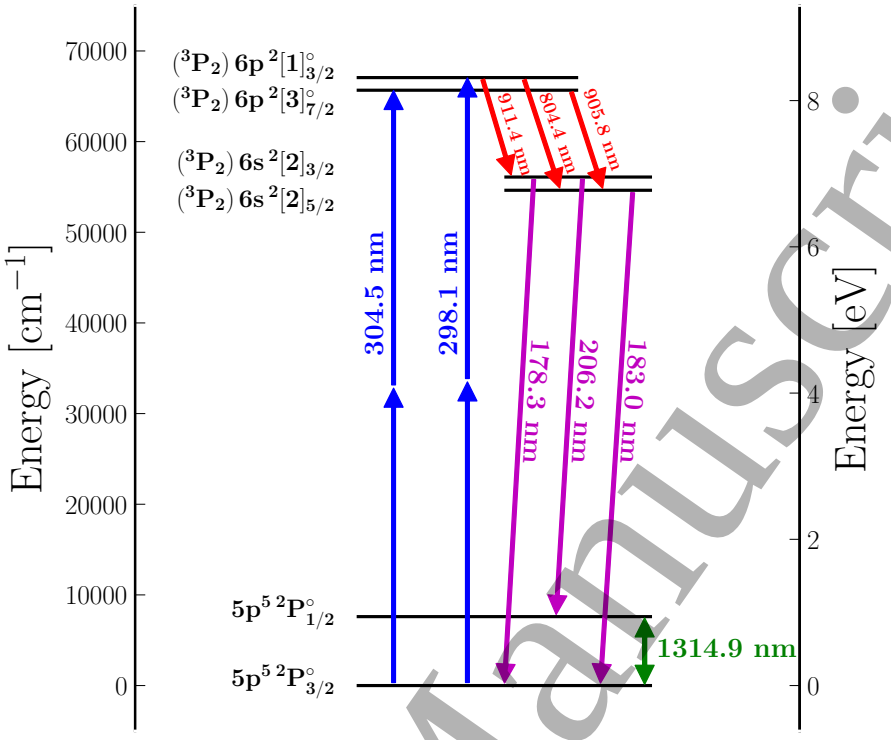

Figure 2. Energy levels of atomic iodine, with the two-photon absorption and infrared fluorescence transitions used in the experiment. For the upper excited $(^3P_2)6p\,^2[1]^\circ_{3/2}$ level, a very weak de-excitation transition to the $(^3P_1)6s\,^2[1]_{3/2}$ level, in the infrared ($\approx 1.907\,\mu$m), has not been represented. Doppler-free two photon spectroscopy makes it possible to revisit the absolute energies of the 6s and 6p levels, the recommended values of which have relied entirely on the spectroscopy of the 183 nm line, as measured in 1959. More precise spectroscopy of the 206 nm line, together with a very accurate measurement of the ground term 7603 cm^{-1} fine structure carried out in 1973, could already suggest that the absolute energies of the upper levels had been overestimated by 0.12(9) cm^{-1}. This is confirmed by the present study, which leads to the more accurate recommendation to revise of all upper energy levels of I I downwards, by -0.169(11) cm^{-1}.

frequency-doubled Nd:YAG laser (Quantel CFR200). The laser line-width, in the Fourier-transform limited regime, i.e. only limited by the finite duration of the pulse (about 6 ns), was about 25 MHz FWHM. The pulsed laser delivered 10 mJ pulses in the near infrared, which, after a stage of frequency doubling in a $5 \times 5 \times 10$ mm^3 AR-coated BBO crystal ($\theta = 25.6\,°$, $\phi = 0\,°$), produced radiation around 450 nm with an energy of about 2 mJ. Summation of the primary and secondary radiations in a $4 \times 4 \times 10$ mm^3 AR-coated BBO crystal ($\theta = 38.3\,°$, $\phi = 90\,°$) produced 300 nm pulses with an energy of about 1 mJ. Even though frequency conversion makes the emission spectral width larger, the output remains essentially Fourier-transform limited, as demonstrated, for double frequency-doubling, by investigation of the 2-photon fundamental $\rightarrow$ $2p^3 3p\,^3P_2$ resonance in O I (Lottigier et al. 2019).

The generated beams were spatially separated using a fused-silica Pellin-Broca

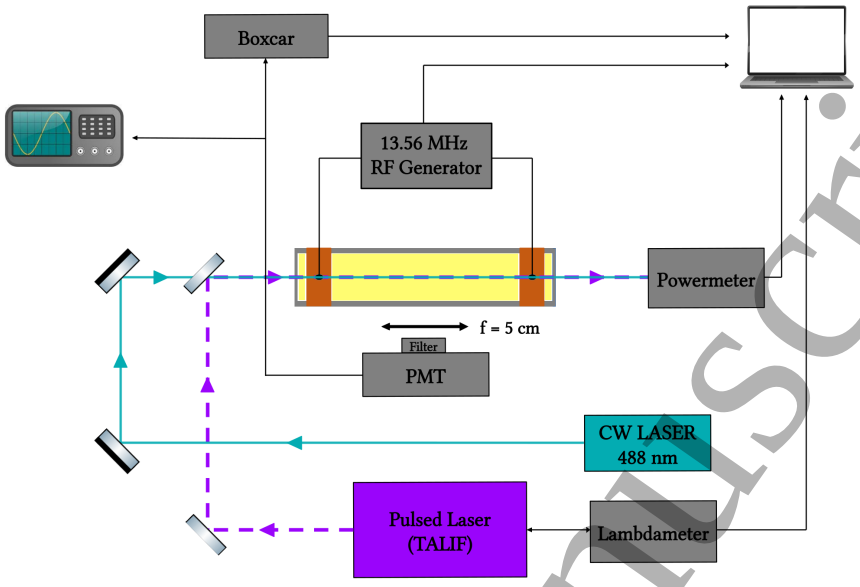

Figure 3. Experimental setup schematics.

prism and the UV light was reflected by dielectric mirrors coated for the UV. In the cell, the size of the ultraviolet beam, as imaged by a UV camera beam profiler (Thorlab - BC106N-UV/M), was $1.28 \times 1.15\,\mathrm{mm}^2$ (figures are for radii at $1/e^2$ times the peak intensity). At the output, the energy was recorded for each laser shot with a PC-interfaced laser energy meter (Pulsar from Ophir).

2.2.2. Fluorescence detection. Fluorescence at 804 nm emitted perpendicularly to the laser beam was collected by a lens with a 50 mm focal length (2f/2f configuration), imaged onto a horizontal slit, passed through an interference filter (with a central wavelength of 800 nm and a 40 nm FWHM) to attenuate the background due to plasma emission, and detected with a red-enhanced photomultiplier (PM) (Hamamatsu R3896), with a gated voltage-divider circuit (Hamamatsu C1392-56) to avoid saturation by plasma emission. To compare the fluorescence between 804 and 905 nm, another PM was used (Hamamatsu R5108) with another interference filter (with a central wavelength of 905 nm, 10 nm FWHM). The fluorescence (TALIF) signal was observed with an oscilloscope (Lecroy 6100A) and recorded through a boxcar integrator (Stanford SR 280), with integration over a 200 ns temporal gate for each laser shot. A Labview™ program was used to record the fluorescence intensity, the ultraviolet pulse energy and the seed laser wavelength.

2.3. Atoms produced by photodissociation

An alternative to the production of iodine atoms by a plasma is to use the photodissociation reaction. This method has also been used in our experiments to measure the lifetime of the $(^3P_2)6p\,^2[1]^o_{3/2}$ level (see section 4). Beyond 20,000 cm^{-1}, light absorption in the diffusive part of the molecular spectrum leads to formation of

atom pairs in states $\mathrm{I}(^2\mathrm{P}^{\mathrm{o}}_{3/2})$ + $\mathrm{I}(^2\mathrm{P}^{\mathrm{o}}_{3/2})$ or $\mathrm{I}(^2\mathrm{P}^{\mathrm{o}}_{3/2})$ + $\mathrm{I}(^2\mathrm{P}^{\mathrm{o}}_{1/2})$ (Larsen et al. 1999), with a proportion of atoms in each level that depends on the wavelength (Wiesenfeld & Young 1981, Hunter & Leong 1987). At the pressures used however, the population in the $\mathrm{I}(^2\mathrm{P}^{\mathrm{o}}_{1/2})$ level remains negligible, due to quenching by collisions with molecules (at rate $Q = k \times n$ with k the quenching coefficient and n the molecular density), which leads to fast de-excitation. For I_2 the value of coefficient k, $3.85 \times 10^{-17}\,\mathrm{m^3\,s^{-1}}$, assumed equal to the average value of table 15 of Chichinin (2006), leads to de-excitation rates ranging from 1.5×10^4 to $3 \times 10^5\,\mathrm{s^{-1}}$.

For atoms in the ground state, losses are dominated by wall recombination processes, the rate of which k_{w} makes wall removal of I atoms more important, for the pressures used, than three-body recombination, the rate of which is about $4 \times 10^{-42}\,\mathrm{m^6\,s^{-1}}$ at 23°C (Ip & Burns 1972). The steady-state density [I] of iodine atoms produced is thus given by: $[\mathrm{I}] = 2\sigma\phi[\mathrm{I_2}]/k_{\mathrm{w}}$, where σ is the I_2 absorption cross section, ϕ the photon flux and $[\mathrm{I_2}]$ the molecular density (Katsoprinakis et al. 2016).

Photodissociation is produced by a diode-pumped blue laser (model LBX-488 HPE from Oxxius). This compact $40 \times 40 \times 100\,\mathrm{mm^3}$ continuous-wave laser can emit up to 1 watt at a wavelength centered around 488.9 nm. The central emission wavelength has been measured with a low resolution fibre miniature spectrometer (Flame from Ocean Optics). The wavelength shifts slightly towards the blue when the power is decreased by the electronic controller. The spectral profile is asymmetric, with a FWHM of about 0.5 nm. The laser beam shape is asymmetric and multimode. We recorded its profile at the centre of the cell, after 105 cm of propagation, with a BC106N-UV - CCD camera beam profiler (Thorlabs). The profile of the beam is mostly flat, with a "top-hat" shape, and its dimensions are $6 \times 1\,\mathrm{mm^2}$. The laser power is stabilized by an internal photodiode.

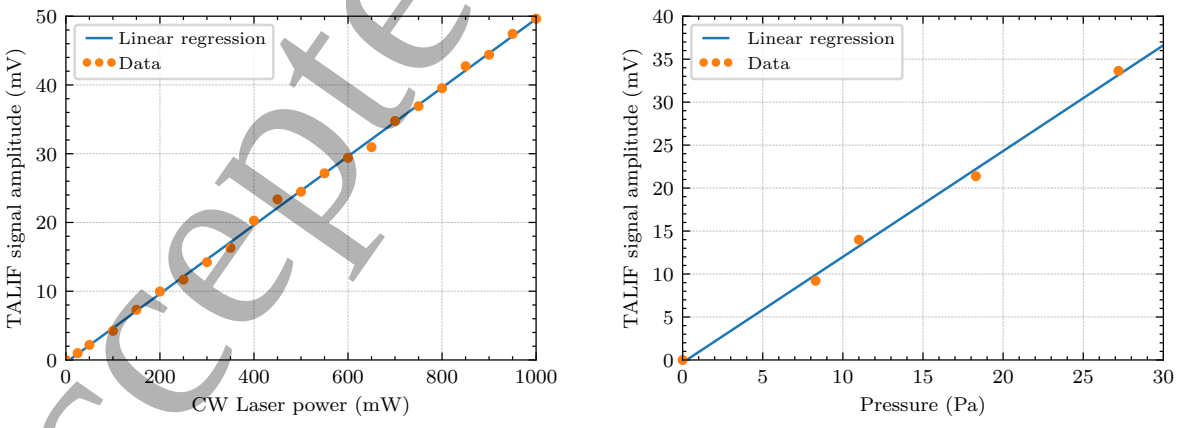

Figure 4. Amplitude of the TALIF signal at the $(^3\mathrm{P}_2)6\mathrm{p}\,^2[1]^{\mathrm{o}}_{3/2}$ resonance (i.e. at a laser wavenumber $\sigma_{\mathrm{L}} = 3 \times 11176.9940\,\mathrm{cm^{-1}}$), recorded following molecular photodissociation. Left: as a function of CW laser power, for a pressure of 28.4 Pa, an energy of the pulsed laser of 320 μJ and a detection voltage $\mathrm{V_{PM}} = 0.65$ kV. Right: as a function of pressure, for a CW power of 1 W, an energy of the pulsed laser of 160 μJ and a detection voltage $\mathrm{V_{PM}}$=0.7 kV. The signals were averaged over 10 shots.

The photodissociation laser is superimposed on the TALIF laser, with the last dichroic microir, R_{max} around 300 nm, allowing the wavelength 488 nm to pass (cf. figure 3). We detected the photodissociation-produced ground state atoms by TALIF following $^2P^o_{3/2} \rightarrow (^3P_2)6p\,^2[1]^o_{3/2}$ excitation. Figure 4 shows the evolution of the integrated TALIF signal as a function of the power of the photodissociation laser or of pressure, i.e. the molecular density. In both cases, the linear variation of the signal confirms that the dominant term for atom loss is the k_w term.

3. Atomic spectroscopy and temperature measurements

The temperature of the ground state atoms can be measured by TALIF spectroscopy using the Doppler broadening of the observed absorption profile. For this application iodine has two disadvantages: it is a heavy atom, the spectroscopic lines of which thus undergo relatively little Doppler broadening, and it has multiple transitions due to its hyperfine structure (linked to the nuclear spin $I = 5/2$ of the only naturally occurring isotope ^{127}I). One must thus disentangle the hyperfine structure from the Doppler-broadened profiles, in order to get unbiased temperature measurements. As a preliminary matter, the use of a high-resolution pulsed laser makes it possible to check the hyperfine structure quantitatively, both as concerns the positions and the relative intensities of the hyperfine components, by Doppler-free two-photon spectroscopy.

3.1. Doppler-free two-photon spectroscopy

When a gaseous sample is illuminated by two counter-propagating beams produced by the same laser, which can be obtained by placing a mirror at the exit of the tube in order to reflect the beam along its original path, absorption of one photon from each beam leads to two-photon excitation with fully compensated 1st-order Doppler shifts, with all velocity classes contributing at the same resonance frequency. This gives rise to a Doppler-free narrow resonance, the width of which reduces to the natural width (Biraben et al. 1974). In a plasma, this homogeneous bandwidth can be increased, however, by collisional dephasing, as observed, for example, in an oxygen glow discharge (Lottigier et al. 2019).

The Doppler-free resonance signal appears superimposed on the ordinary Doppler-broadened profile that corresponds to absorption of two photons from the same beam. Figure 5 shows two Doppler-free spectra centered around the resonances from the ground $5s^25p^5\,^2P^o_{3/2}$ to the $(^3P_2)6p\,^2[1]^o_{3/2}$ and $(^3P_2)6p\,^2[3]^o_{7/2}$ levels, respectively.

3.2. Absolute energy of the excited states

Doppler-free spectroscopy reveals the hyperfine structure of the $^2P_{3/2} \rightarrow (^3P_2)6p\,^2[1]^o_{3/2}$ and $^2P_{3/2} \rightarrow (^3P_2)6p\,^2[3]^o_{7/2}$ lines, which is found to agree perfectly with the structure that has been well-known after repeated hyperfine investigations (Jaccarino et al. 1954, Luc-Koenig et al. 1973, Luc-Koenig et al. 1975, Mu et al. 2018, Ashok et al. 2019).

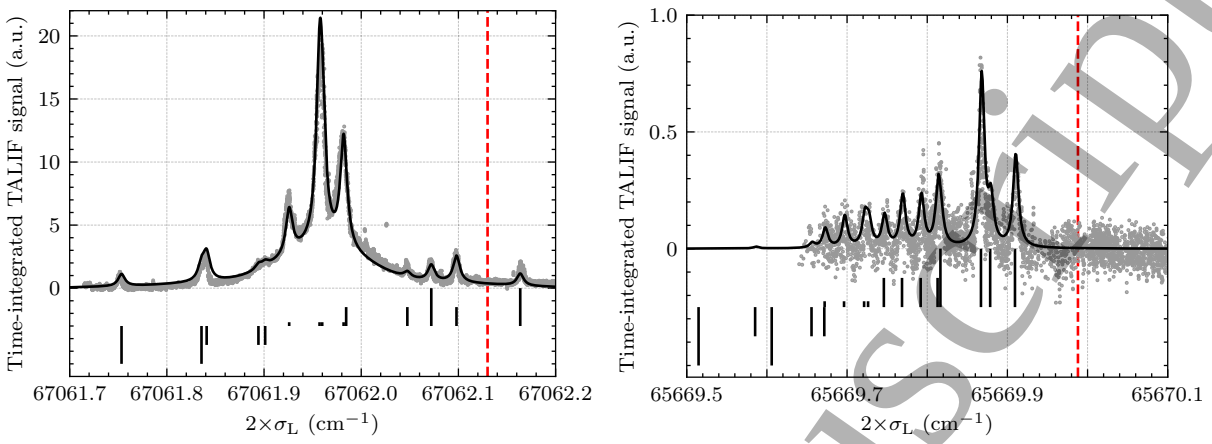

Figure 5. Fluorescence spectra in Doppler-free configuration, as functions of the excitation wavenumber, i.e. twice the laser wavenumber σ_L. Left: time-integrated fluorescence following excitation of the $(^3P_2)6p\,^2[1]^o_{3/2}$ level of I around 67062.130 cm^{-1}. The atoms are produced in a plasma excited by a RF power of 20 W with an initial pressure of 5 Pa and detected with an R3896 photomultiplier (PMT). The data points are fitted by the sum (continuous line) of a Doppler-free and a Doppler-broadened hyperfine multiplet, the former with a homogeneous linewidth of 0.0082 cm^{-1} and the latter assuming a translational temperature of 530 K. The larger integrated area of the Doppler-broadened profile comes from imbalance between the counter-propagating beams, which increases the probability of having two photons absorbed from the same beam. The best-fitting value of the isotropic-to-quadrupole excitation ratio was found equal to 4.25 ± 0.5 (see text). Right: time-integrated fluorescence following two-photon excitation of the $(^3P_2)6p\,^2[3]^o_{7/2}$ level of I around 65669.988 cm^{-1}, with a RF excitation power of 40 W and an initial pressure of 25 Pa, as seen through an RR5108 PMT detector. Absence of an isotropic component maybe an explanation for the much lower intensity of that transition. An advantage of $\Delta J \neq 0$ transitions, however, is that the overall amplitude remains the only adjustable parameter when fitting the calculated profile (continuous line) to the data. For every spectrum, the expected mean position of the transition is represented by a vertical dashed line, at the tabulated energy (Kramida et al. 2021). The black vertical segments show the positions of the hyperfine transitions, with a height proportional to the change ΔF of total angular momentum, in the [-2 ..+2] interval. In both cases, the hyperfine multiplet experimentally appears globally red-shifted by -0.169 cm^{-1}, with respect to the position given by the NIST atomic spectra database (Luc-Koenig et al. 1975, Kramida et al. 2021).

However, fitting the expected multiplet to the observed structure reveals a global shift of both lines by -0.169 cm^{-1} with respect to the energies of the atomic spectra database of the National Institute of Standards and Technology (NIST) (Kramida et al. 2021). This shift is determined with a pointing accuracy of ± 0.001 and ± 0.002 cm^{-1} for the $6p\,^2[1]^o_{3/2}$ and the $6p\,^2[3]^o_{7/2}$ level, respectively, to which must be added the uncertainty of the energy calibration process.

In the following, we shall endeavour to provide the reader with uncertainties that can be relied on to ascertain that future, more precise measurements will find the wavenumbers at stake within the proposed intervals, with a high level of confidence.

That means understanding those uncertainties, if they are to be interpreted as statistical uncertainties, as expanded ones. One should keep in mind, however, that the uncertainties provided by past literature may not have included the minimum factor of 2 needed, when translating standard deviations into expanded uncertainties. As the present work has included all historical sources, the uncertainties of which often appear elusive, dividing the uncertainties finally obtained in the present study by a factor of 2 to get a final 'standard deviation' may prove dangerously overoptimistic, especially due to the scarcity of some data and the possibility of systematic effects that can affect all wavenumbers together (which would ruin all statistical interpretations). One can have a high level of confidence - no more no less - in finding the actual wavenumbers within the indicated intervals.

As already mentioned in section 2.2.1, the lambdameter used for wavelength measurements was calibrated daily with a saturated-absorption stabilized diode laser, using the $6s\,^2S_{1/2}\,F = 4 \rightarrow 6p\,^2P^o_{3/2}\,F' = 5$ component of the D2 line of cesium at 852.1 nm. Reliability of that calibration at remote wavelengths was checked by measuring the position of two hyperfine components of the D1 transition, the wavelength of which, ca 894.3 nm, offers the advantage of being very close, in the infrared, to the wavelength of 894.6 nm generated, before frequency tripling, for $5s^25p^5\,^2P^o_{3/2} \rightarrow (^3P_2)6p\,^2[1]^o_{3/2}$ two-photon excitation of iodine. The offset between the reference and measured frequencies was no more than 15 MHz. Another effect to consider is a possible frequency shift of the injected pulsed laser relative to the measured frequency of the CW seeder. Heterodyne measurements made it possible to check that the pulsed laser mean output frequency is equal to that of the seed laser to within 20 MHz and may drift by 20 MHz during the pulse (Cabaret & Drag 2010). The sum of these three contributions gives a possible systematic error of $15 + 20 + 20 = 55$ MHz. The tripled frequency thus appears determined with an uncertainty of 165 MHz and the precision of the measured frequency of the two-photon transition around 65000 cm^{-1} is 330 MHz, i.e. 0.011 cm^{-1}.

As for the existing data on the excited levels of atomic iodine, the relative energies of the levels between 50000 and 80000 cm^{-1} have reached a precision of 0.005 cm^{-1}, thanks to infrared Fourier-transform (IR-FT) spectroscopy (Luc-Koenig et al. 1975). The same study also provided the magnetic dipole and electric quadrupole hyperfine structure parameters of 37 even levels and 42 odd levels. The atomic energy levels that we shall discuss are the barycenters of the hyperfine multiplets.

IR spectroscopy, however, cannot determine energies with respect to the atomic ground level and it was thus a misinterpretation to assign the same $\pm 0.005\,cm^{-1}$ precision to the absolute energies of the excited states, when these energies have just been calculated by addition of the suitable IR intervals to the baseline energy of all excited configurations, namely the energy of the $(^3P_2)6s\,^2[2]_{5/2}$ level, numerically 54633.46 cm^{-1}, as given by the 1962 review (Minnhagen 1962).

Table 1 shows the best estimates of the energies of the ground configuration, of the $(^3P_2)6s\,^2[2]$ term and of the two levels that we have experimentally studied, before and after the IR-FT measurements (Luc-Koenig et al. 1973, Luc-Koenig et al. 1975)

Table 1. Successive optimizations of the energy levels of atomic iodine, from left to right, first according to the 1962 data, then according to the present NIST database, including the infrared Fourier-transform (IRFT) measurements and, finally, taking the TALIF-measured energies of the $(^3P_2)6p\,^2[1]^o_{3/2}$ and $(^3P_2)6p\,^2[3]^o_{7/2}$ levels into account. The 1975 data could have led to the conclusion that all excited levels of I I had to be shifted by $-0.12(9)\,cm^{-1}$. Our TALIF measurements make the recommendation more precise: with the exception of the first fine-structure excited level, all excited levels have to be shifted by $-0.169(11)\,cm^{-1}$ (with a slightly smaller or larger uncertainty depending on the more or less direct character of their spectroscopic connection to the directly accessed levels).

Term	J	UV & VUV[a]	NIST[b]	+IR-FT[c]	+TALIF[d]
$5s^25p^5\ ^2P^o$	3/2	0.00	0.000	0.000	0.000
	1/2	7603.15(17)	7602.970(5)	7602.9765(5)	7602.9765(5)
$5s^25p^4(^3P_2)6s\ ^2[2]$	5/2	54633.46(15)	54633.460	54633.34(9)	54633.291(11)
	3/2	56092.88(15)	56092.881	56092.76(8)	56092.713(15)
$5s^25p^4(^3P_2)6p\ ^2[3]^o$	7/2	65669.99(16)	65669.988	65669.86(9)	**65669.819**(11)
$5s^25p^4(^3P_2)6p\ ^2[1]^o$	3/2	67062.07(15)	67062.130	67062.01(9)	**67061.961**(10)

[a]With only the data of UV and VUV spectroscopy (Kiess & Corliss 1959, Minnhagen 1962); [b]As presently given by the NIST (Kramida et al. 2021); [c]With the output of infrared Fourier-Transform spectroscopy added to the former data (Luc-Koenig et al. 1975, Engleman et al. 1980, Cerny et al. 1991); [d]With the present two-photon spectroscopy results (in bold) added to all former data.

and, finally, when the data obtained in the present investigation are taken into account in a consistent optimization, using the standard methods of atomic spectroscopy (Kramida 2011, Blondel 2020). Even though a rigorous optimization shall include every experimentally known level of iodine, all upper intervals are so tightly constrained by the results or IR-FT spectroscopy that, with the precision limit of $\pm 0.011\,cm^{-1}$ set by our photo-excitation scheme, the whole spectroscopic problem appears summarized in the optimization of those five levels.

The $54633.46\,cm^{-1}$ energy of the $(^3P_2)6s\,^2[2]_{5/2}$ level (Minnhagen 1962, Luc-Koenig et al. 1975, Kramida et al. 2021), which, as we have just said, serves as the baseline for the upper part of the spectrum, comes from vacuum ultra-violet (VUV) spectroscopy of the corresponding resonance line, which yielded a wavelength of 183.0380 nm (Kiess & Corliss 1959).

Knowing the fine-structure interval of the $(^3P_2)6s\,^2[2]$ doublet from spectroscopy of the upper transitions related to both its $J = 5/2$ and $J = 3/2$ states, one can deduce the $(^3P_2)6s\,^2[2]_{5/2} - 5p^5\,^2P^o_{1/2}$ interval from the measurement of the 206.1633 nm wavelength of the $(^3P_2)6s\,^2[2]_{3/2} - 5p^5\,^2P^o_{1/2}$ transition, which has been attributed a $48489.73\,cm^{-1}$

wavenumber. The difference provides a measure of the fine structure interval of the ground term, 7603.15 cm^{-1} (Kiess & Corliss 1959), which was the value retained in the 1962 review of the I I spectrum (Minnhagen 1962).

However, this 7603.15 cm^{-1} value of the ground term $^2\mathrm{P}^\mathrm{o}_{1/2} - {}^2\mathrm{P}^\mathrm{o}_{3/2}$ fine-structure interval appeared but marginally compatible with the 7602.7 cm^{-1} value that had been repeatedly published by Murakawa (Murakawa 1938, Murakawa & Suwa 1954, Murakawa 1958), as with the independent measurement of a wavenumber of $7605.03 \pm 0.1\,\mathrm{cm}^{-1}$ in air, i.e. $7602.95 \pm 0.1\,\mathrm{cm}^{-1}$ in vacuum (Eshbach & Fisher 1954). Another value of the same interval could be deduced from the wavenumbers of the $(^3\mathrm{P}_2)7s\,{}^2[2]_{3/2} - 5p^5\,{}^2\mathrm{P}^\mathrm{o}_{3/2}$ and $(^3\mathrm{P}_2)7\mathrm{s}\,{}^2[2]_{3/2} - 5p^5\,{}^2\mathrm{P}^\mathrm{o}_{1/2}$ transitions, as measured by Martin (Minnhagen 1962), and even though the uncertainty of the corresponding $72294.1 - 64692.1 = 7602.0\,\mathrm{cm}^{-1}$ difference must be of the order of $1\,\mathrm{cm}^{-1}$, it also suggested that the 7603.15 cm^{-1} value could be slightly overestimated. That was confirmed by IR-FT spectroscopy, which found a mean fine-structure interval of $7602.977(3)\,\mathrm{cm}^{-1}$ (Luc-Koenig et al. 1973), i.e. a value lower by $0.180\,\mathrm{cm}^{-1}$ (sic) than the one deduced from VUV spectroscopy (Kiess & Corliss 1959). The figure was later consolidated to $7602.976(1)\,\mathrm{cm}^{-1}$ (Engleman et al. 1980), then $7602.9765(5)\,\mathrm{cm}^{-1}$ (Cerny et al. 1991), but it must be kept in mind that this is only the centroid of a more than $0.6\,\mathrm{cm}^{-1}$ wide $^2\mathrm{P}^\mathrm{o}_{1/2} - {}^2\mathrm{P}^\mathrm{o}_{3/2}$ hyperfine multiplet. As a consequence, precise spectrometry of the lines connected to the $^2\mathrm{P}^\mathrm{o}_{1/2}$ level can remain especially difficult, when the hyperfine structure is not resolved.

Precise measurement of the fine-structure interval of the ground term does not give immediate information on the energy of higher-excited levels, anyway. It tells a lot, however, on what the uncertainty of VUV spectroscopy at 178 and 183 nm must have been, to make a VUV-wavenumber difference miss the accurate value later obtained by IR-FT spectroscopy by $0.18\,\mathrm{cm}^{-1}$. As the 206 nm line was measured with a greater care and "relative to international secondary standards in the iron arc spectrum" (Kiess & Corliss 1959), while the 178 and 183 nm wavelengths were measured in a less direct way "making use of the combination principle", attributing uncertainties of 0.09 and $0.2\,\mathrm{cm}^{-1}$ to the 206 nm and VUV lines, respectively, appears reasonable and consistent with subsequently found corrections. Smaller uncertainties, taking into account all data described above but ours, would make some corrections of the energies of the first three excited levels of I I exceed the assumed standard deviation. On that sole basis, standard optimization of the energy levels already leads to recommend a revision of the energy of the $(^3\mathrm{P}_2)6\mathrm{s}\,{}^2[2]_{5/2}$ level, hence of the energies of all upper levels, as shown in the penultimate column of table 1, by $-0.12(9)\,\mathrm{cm}^{-1}$. At this stage, the associated uncertainty still appears nearly as large as the proposed correction, but the recommendation already implies that the upper energy levels of I I lie well below the $\pm 0.005\,\mathrm{cm}^{-1}$ uncertainty intervals that have been spuriously attached to them in the NIST data table (Kramida et al. 2021).

Much more information is brought forward by our observation of a $-0.169(11)\,\mathrm{cm}^{-1}$ shift of the two studied levels of the $(^3\mathrm{P}_2)6\mathrm{p}$ configuration. Injection of their updated

positions into the energy level-optimization algebra makes the shift of the whole upper spectrum much more precise, with recommended corrections all close to the same $-0.169(11)\,\mathrm{cm}^{-1}$ value. At this point, one can remark that since the wavenumbers associated to the 178 nm and 183 nm lines directly determine the energies of the $(^3\mathrm{P}_2)6\mathrm{s}\,^2[2]$ doublet, their uncertainty could not have been smaller in absolute value, which appears consistent with our assumption of a $0.2\,\mathrm{cm}^{-1}$ uncertainty, but invalidates the claim that the VUV wavelengths were "correct to less than 0.005 Å" (Kiess & Corliss 1959). As a matter of fact, the final correction appears no smaller than +0.0057 Å as concerns the 183 nm line.

Concurrently, the wavenumber of the 206 nm line, which had appeared changed from the original $48489.73\,\mathrm{cm}^{-1}$ (Kiess & Corliss 1959) to a strikingly different $48489.911\,\mathrm{cm}^{-1}$ in the NIST table (Kramida et al. 2021), gets restored to a $48489.736(15)\,\mathrm{cm}^{-1}$ value much closer to the original one. The fact the associated correction drops back to $0.006\,\mathrm{cm}^{-1}$, i.e. only a fraction of the $0.09\,\mathrm{cm}^{-1}$ uncertainty that we have attached to it, may be regarded as a demonstration of the consistency of the spectrometry of the 206 nm line (Kiess & Corliss 1959), the accurate measurements of the ground-term fine structure (Luc-Koenig et al. 1973, Engleman et al. 1980, Cerny et al. 1991) and the present laser-spectroscopy measurements of the $(^3\mathrm{P}_2)6\mathrm{p}\,[1]^\mathrm{o}_{3/2}$ and $(^3\mathrm{P}_2)6\mathrm{p}\,[3]^\mathrm{o}_{7/2}$ wavenumbers. Pending a new global optimization of the energy levels of I I, we can already conclude by recommending that all excited levels of iodine, starting from the $5s^25p^4(^3\mathrm{P}_2)6\mathrm{s}\,^2[2]_{5/2}$, be shifted by $-0.169\,\mathrm{cm}^{-1}$ and that none of their absolute energies be attributed a precision better than $\pm 0.01\,\mathrm{cm}^{-1}$.

3.3. Relative intensities of two-photon transitions

3.3.1. Relative intensities of hyperfine components. Disentangling the hyperfine structure from the Doppler-broadened profile does not only require knowing the relative positions of the hyperfine components. It also requires knowing their relative intensities. These relative intensities can be derived from the observation that the two-photon excitation amplitude contains two terms, given by the reduced matrix elements of tensor operators $Q^{(k)}$, the rank k of which can be 0 or 2. These two terms, to be named the scalar (or isotropic) and quadrupolar term, respectively, contribute to every hyperfine component by relative intensities (Grynberg et al. 1976, Flusberg et al. 1976, Grynberg et al. 1977, Grynberg & Cagnac 1977)

$$I_k(F_\mathrm{g},F_\mathrm{e}) \propto (2F_\mathrm{g}+1)(2F_\mathrm{e}+1) \begin{Bmatrix} J_\mathrm{e} & J_\mathrm{g} & k \\ F_\mathrm{g} & F_\mathrm{e} & I \end{Bmatrix}^2 \frac{\left|\left\langle \mathrm{e}J_\mathrm{e}||Q^{(k)}||\mathrm{g}J_\mathrm{g}\right\rangle\right|^2}{2k+1} \sum_q \left|a_q^{(k)}\right|^2 \qquad (1)$$

where J_g and F_g are the electron and total angular momenta of the ground level, and J_e and F_e are those of the excited level, respectively. The $a_q^{(k)}$ coefficients characterize the relative polarizations of the two absorbed photons in such a way that when the two

absorbed photons have the same linear polarization, $\left|a_0^{(0)}\right|^2$ and $\sum_q \left|a_q^{(2)}\right|^2$ are just 1/3 and 2/3, respectively.

So when the observed distribution of relative intensities is reproduced, with adjustable α_k coefficients, by a combination such as

$$(2F_\mathrm{g}+1)(2F_\mathrm{e}+1)\sum_{k=0,2}\alpha_k \begin{Bmatrix} J_\mathrm{e} & J_\mathrm{g} & k \\ F_\mathrm{g} & F_\mathrm{e} & I \end{Bmatrix}^2 \sum_q \left|a_q^{(k)}\right|^2 \qquad (2)$$

the α_0/α_2 ratio gives a measure of $5 \times \left|\left\langle \mathrm{e}J_\mathrm{e}||Q^{(0)}||\mathrm{g}J_\mathrm{g}\right\rangle\right|^2 / \left|\left\langle \mathrm{e}J_\mathrm{e}||Q^{(2)}||\mathrm{g}J_\mathrm{g}\right\rangle\right|^2$.

Yet reduced matrix elements $\left\langle \mathrm{e}J_\mathrm{e}||Q^{(k)}||\mathrm{g}J_\mathrm{g}\right\rangle / \sqrt{2k+1}$ are sums of second-order products of one-photon transition amplitudes over all possible intermediate states $|\mathrm{r}J_\mathrm{r}\rangle$ that can link a ground state $|\mathrm{g}J_\mathrm{g}\rangle$ to an excited state $|\mathrm{e}J_\mathrm{e}\rangle$ and, inside these sums, the k-dependence is just given by a $\begin{Bmatrix} J_\mathrm{e} & J_\mathrm{g} & k \\ 1 & 1 & J_\mathrm{r} \end{Bmatrix}$ coefficient (Grynberg & Cagnac 1977). If it thus happens that only one intermediate level (or, at least, only one J_r value) determines the value of the two-photon amplitude, the α_0/α_2 ratio will be just the squared ratio of the corresponding 6-j symbols. Given the fact that the question of the isotropic-to-quadrupolar ratio arises only if $J_\mathrm{e} = J_\mathrm{g}$ and the simple expression of 6-j symbols when one of the j values (here k) is zero, that would lead to a purely angular ratio

$$\frac{\alpha_2}{\alpha_0} = 3(2J_\mathrm{g}+1)\begin{Bmatrix} J_\mathrm{g} & J_\mathrm{g} & 2 \\ 1 & 1 & J_\mathrm{r} \end{Bmatrix}^2 \qquad (3)$$

Unfortunately, excitation from the ground to the $(^3\mathrm{P}_2)6\mathrm{p}\,^2[1]^\mathrm{o}_{3/2}$ level of iodine (the only one of the two studied that calls for an assessment of the scalar-to-quadrupolar ratio) can go through intermediate states of several possible J_r values. Just considering the states with an energy between the ground and the excited level, the $(^3\mathrm{P}_2)6\mathrm{s}\,^2[2]_{3/2}$ and $(^3\mathrm{P}_2)6\mathrm{s}\,^2[2]_{5/2}$ states seem to be nearly as favorably positioned, as concerns the energy defect with respect to one-photon resonance. With the one or the other possible value of $J_\mathrm{r} = 3/2$ or $5/2$, equation (3) would lead to a ratio α_0/α_2 of 25/8 or 50, respectively. The experimental value found by fitting the experimentally recorded profile with formula (2), as shown in figure 5, is 4.25 ± 0.5, which may suggest that the transition amplitude gets its larger contribution from the $J_\mathrm{r} = 3/2$ intermediate states.

Anyway, obtaining a very satisfactory agreement of the calculated and actually recorded hyperfine structures with only that single adjustable parameter (or, in the case of the purely quadrupolar $^2\mathrm{P}_{3/2} \rightarrow (^3\mathrm{P}_2)6\mathrm{p}\,^2[3]^\mathrm{o}_{7/2}$ transition, with no adjustable parameter at all) shows how reliably pure Doppler contribution can be extracted from the composite Doppler-broadened profile, for temperature measurements. That will be illustrated in section 3.4.

3.3.2. Dominance of $\Delta F = 0$ and $\Delta J = 0$ components? In the above example, the contribution of the isotropic term has appeared as the dominant one, for the two-

photon transitions where a scalar contribution is allowed, i.e. when $F_e = F_g$, if $J_e = J_g$. This may suggest that the larger intensity observed in iodine for the excitation of the $(^3P_2)6p\,^2[1]^o_{3/2}$, when compared to excitation of the $(^3P_2)6p\,^2[3]^o_{7/2}$ level as shown in figure 5, follows from a general rule, according to which $\Delta J = 0$ two-photon transitions would be especially intense ones. The hypothesis may seem substantiated by our finding that the excitation cross-section from the ground $J=0$ state to a $J=0$ level was larger than to a $J = 2$ level of the same configuration in xenon (Drag et al. 2021). Yet in this latter case the situation was more clear-cut, for starting from a $J_g = 0$ state even made the transition to a $J_e = 0$ state a pure isotropic one. However, much smaller values of the α_0/α_2 ratio were found in neon (Grynberg et al. 1977) and in europium (Kronfeldt & Loa 1992), which shows that having larger isotropic contributions than their quadrupolar counterparts cannot be considered as a general rule.

3.3.3. Relative intensities of LS fine structure components obey the same formulas. Meanwhile isotropic reinforcement may be regarded as the reason that makes $\Delta J = 0$ components the most intense ones in two-photon excitation between the ground $2p^4\,{}^3P$ and excited $2p^3\,3p\,{}^3P$ terms of atomic oxygen (Bamford et al. 1987). In the same way as the relative intensities of hyperfine components can be accounted for by formula (1), the relative intensities of fine structure components of a two-photon, electric dipole transition with no change in the total spin state (which is mandatory in pure LS coupling) are expected to follow an intensity distribution

$$I(J_g, J_e) \propto (2J_g+1)(2J_e+1) \sum_{k=0,2} \begin{Bmatrix} L_e & L_g & k \\ J_g & J_e & S \end{Bmatrix}^2 \frac{\left|\langle e L_e || Q^{(k)} || g L_g \rangle\right|^2}{2k+1} \sum_q \left|a_q^{(k)}\right|^2 \quad (4)$$

with L_g and L_e the orbital angular momentum of the ground and excited level, respectively, and S the total, invariant, spin. Only do transitions such that $J_e = J_g$ include a scalar $k = 0$ contribution and these transitions actually appear as the most intense ones, in the set of $2p^4\,{}^3P \rightarrow 3p\,{}^3P$ two-photon transitions (Bamford et al. 1987). On the other hand, the relative intensities of purely quadrupolar transitions can be predicted straight away to be proportional to the angular factor $(2J_g+1)(2J_e+1)\begin{Bmatrix} L_e & L_g & 2 \\ J_g & J_e & S \end{Bmatrix}^2$, i.e. $(2J_g+1)(2J_e+1)\begin{Bmatrix} 1 & 1 & 2 \\ J_g & J_e & 1 \end{Bmatrix}^2$ for the said transition in oxygen. This is exactly what Saxon & Eichler remarked, when they observed that their detailed calculation provided two-photon excitation cross-sections $\sigma_{0\to2}$, $\sigma_{1\to2}$, $\sigma_{2\to1}$ and $\sigma_{2\to0}$ in the same ratios as 20/9, 5/3, 1 and 4/9, respectively (Saxon & Eichler 1986), taking into account the fact that a cross-section must be written without the $(2J_g+1)$ front factor, for the concept of a cross-section applies to an individual atom in a well-defined initial state, not to the degeneracy-amplified population of a statistical sample. And the observation that "each spectrum [spanning all three possible J_e values] has the same integrated area", whatever the J_g initial value

(Bamford et al. 1987), which already appeared in the calculations of the fine-structure components of the cross-section (Pindzola 1978, Crosley & Bischel 1984), is just an illustration of the symmetry made tangible by the orthonormalization of 6-j symbols: whatever the J_g value, for every k

$$\sum_{J_e} (2J_e + 1) \begin{Bmatrix} L_e & L_g & k \\ J_g & J_e & S \end{Bmatrix}^2 = \frac{1}{2L_g + 1} \tag{5}$$

which, for a $^3\mathrm{P} \rightarrow ^3\mathrm{P}$ transition, is just 1/3.

3.4. Temperature measurement and relative density

For temperature measurements, we have probed the most favorable transition for two-photon excitation that can be reached with our laser system, namely to the $(^3\mathrm{P}_2)6\mathrm{p}\,^2[1]^\mathrm{o}_{3/2}$ level. We also checked the quadratic dependence of the TALIF signal on the laser intensity in the perturbative regime, with an energy not exceeding 400 μJ and using a collimated beam. Focusing the laser beam with a 200 mm lens makes higher-order non-linear phenomena appear, like amplified spontaneous emission or photo-ionization, as well as a TALIF signal even in the absence of plasma excitation, due to molecular photo-dissociation. In the latter condition, the dependence of the TALIF signal on energy saturates.

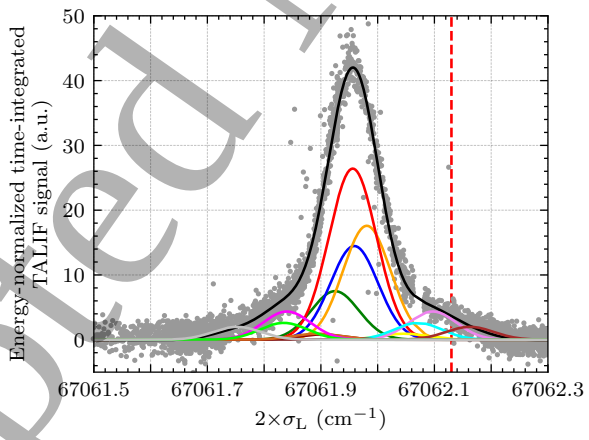

Figure 6. Laser squared energy-normalized TALIF response of the I $5\mathrm{p}^5\,^2\mathrm{P}^\mathrm{o}_{3/2} \rightarrow (^3\mathrm{P}_2)6\mathrm{p}\,^2[1]^\mathrm{o}_{3/2}$ line in a discharge established with an initial pressure p=6.2 Pa and an input RF power of 40 W, as a function of the excitation wavenumber, i.e. twice the laser wavenumber σ_L. The raw data points are shown together with a multi-peak Gaussian fit (each colour corresponds to one single hyperfine component) calculated with the isotropic-to-quadrupolar α_0/α_2 ratio of 4.25 determined by Doppler-free spectroscopy. The best-fitting temperature appears to be 533 ± 15 K. The found uncertainty must be doubled by another ± 15 K due to the ± 0.5 uncertainty on the α_0/α_2 ratio. The red dashed line is the expected position of the barycenter of the transition (Luc-Koenig et al. 1975, Kramida et al. 2021).

An example of a TALIF profile is given on figure 6. The temperature of the iodine

atoms formed in the RF discharge is determined by a multi-peak Gaussian fit taking the different hyperfine components into account. Evolution of the temperature is shown in figure 7, as a function of the excitation power and for different pressures. The temperature increases with the RF power, and this increase is all the more important as the pressure is higher. It can go up to 1250 K due to the kinetic energy that atoms acquire during molecular dissociation, as already observed in Cl_2 (Cunge et al. 2009).

A measure of the relative density of I atoms in the ground $^2P^o_{3/2}$ level is given by the frequency-integrated value of the TALIF signal, the variation of which as a function of the applied RF power is also shown in figure 7. A scaling factor has been applied to get the same variation close to the origin and compensate for the day-to-day variations of the collection efficiency of the optical detection and of the electronic gain factors. Moreover, the possibility of quenching, which can depend on temperature and thus on power, has not been taken into account. For different pressures, the ground state atoms density saturates for similar values of the RF power, which very likely results from saturation of molecular dissociation in the plasma. All in all, saturation of the signal, larger Doppler broadening with the associated decrease of the peak fluorescence and larger background noise due to plasma emission combine together to deteriorate the signal-to-noise ratio at higher values of the excitation power.

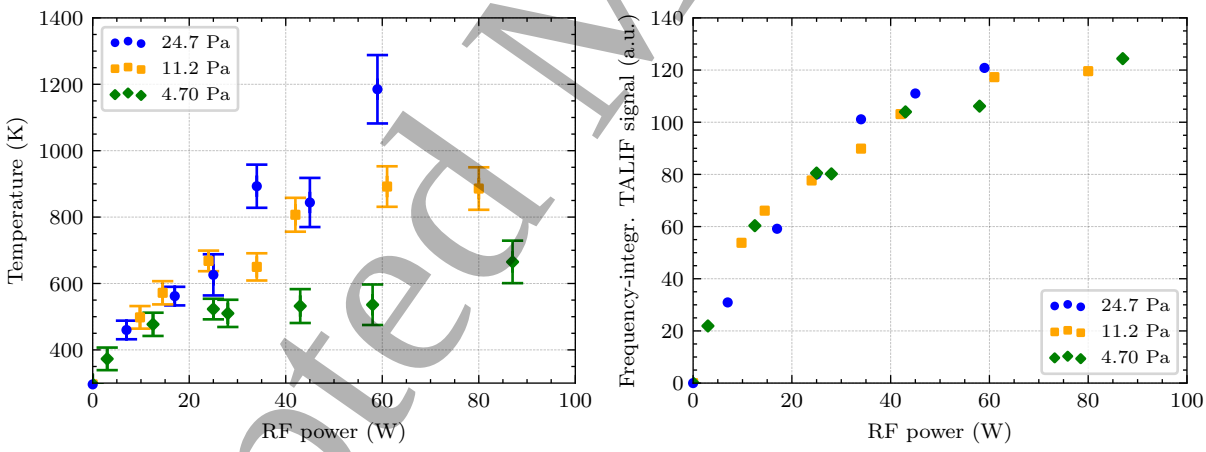

Figure 7. Left: measured atomic gas temperature as a function of RF power for different pressures. Right: Relative frequency-integrated value of the TALIF signal as a function of RF power for different initial pressures.

3.5. I ($^2P^o_{1/2}$) detection

In addition to the very possible saturation of molecular dissociation of I_2, saturation of the increase of the population of atoms in the ground state with RF power, as shown by figure 7), may also be due to some excitation to the upper $5p^5\,^2P^o_{1/2}$ fine-structure component of the atomic ground term, by electron collisions.

Detection of such fine-structure excited iodine atoms was thus attempted, taking the reduction of the excitation energy by the fine structure interval into account. Within

the limits of the wavelengths accessible to our laser system, we tried several excitation schemes - towards the $(^3P_1)6p\,^2[1]^o_{1/2}$, $(^3P_2)7p\,^2[2]^o_{3/2}$ and $(^3P_1)6p\,^2[2]^o_{3/2}$ levels - taking care to adapt the detection settings to each possible fluorescence scheme (which concerns both the filter and detector). We did not observe any signal, which may be due to a relatively high quenching rate of the $^2P^o_{1/2}$ level down to the ground $^2P^o_{3/2}$ level at the densities used or, inclusively, to the weakness of the TALIF transitions chosen for detection.

The latter explanation could be supported by the relative weakness of the 206 nm line, when compared to the much more intense 183 and 178 nm ones (Kramida et al. 2021, Kiess & Corliss 1959, Lawrence 1967, Filin et al. 2020), which reveals larger electric dipole matrix elements to the first, $(^3P_2)6s\,^2[2]$, term starting from the ground level than from the fine-structure excited $^2P^o_{1/2}$. However, even though the $(^3P_2)6s\,^2[2]$ term is the most favorably weighted, as the one closest to one-photon resonance, many more virtual intermediate states contribute to the series of dipole-products that makes the two-photon transition amplitude. A stronger coupling is also expected from the lower, $^2P_{3/2}$, level, when going to the next excited, $(^3P_0)6s\,^2[0]_{1/2}$ level (Lawrence 1967), yet the absolute intensity of the corresponding lines appeared experimentally as rather weak ones, and with similar intensities (Kiess & Corliss 1959). But, just going to the following excited levels, one already finds a coupling to the $(^3P_1)6s\,^2[1]$ doublet stronger from the $^2P^o_{1/2}$ level than from the ground $^2P^o_{3/2}$ one (Kramida et al. 2021, Kiess & Corliss 1959, Filin et al. 2020). In the present state of our knowledge of the I I spectrum, there is thus no reason (apart from the factor of 1/2 given by the degeneracy ratio) to think that the two-photon excitation scheme shall be less efficient for $^2P^o_{1/2}$ than for $^2P^o_{3/2}$ detection.

4. Measurement of the radiative lifetime of the $(^3P_2)6p\,^2[1]^o_{3/2}$ level

In order to measure the lifetime of the $(^3P_2)6p\,^2[1]^o_{3/2}$ states, we could excite to that level atoms produced either in a plasma or by photodissociation, and actually took advantage of the availability of these two methods. In a plasma, the number of atoms can be larger, so the TALIF response is bigger, but the signal is noisier (due to radio frequency excitation), with a larger background due to the electronic excitation of atoms followed by fluorescence. Moreover, as the RF power applied to the plasma increases, the gas heats up, the dissociation rate changes and the quenching coefficient gets modified because it depends on the molecular density. We have therefore limited plasma excitation to very low RF powers (between 2 and 8 watts). When atoms are produced by photodissociation, the signal is not noisy but weaker, because the density of neutral atoms produced is smaller, which limits the pressure range that can be used to above 8 Pa.

Figure 8 shows an example of a TALIF signal record and the way it can be fitted with an exponential decay curve, taking into account both the detector fall time (2.2×1.5 ns) and the transit time spread (1.2 ns) given by the manufacturer.

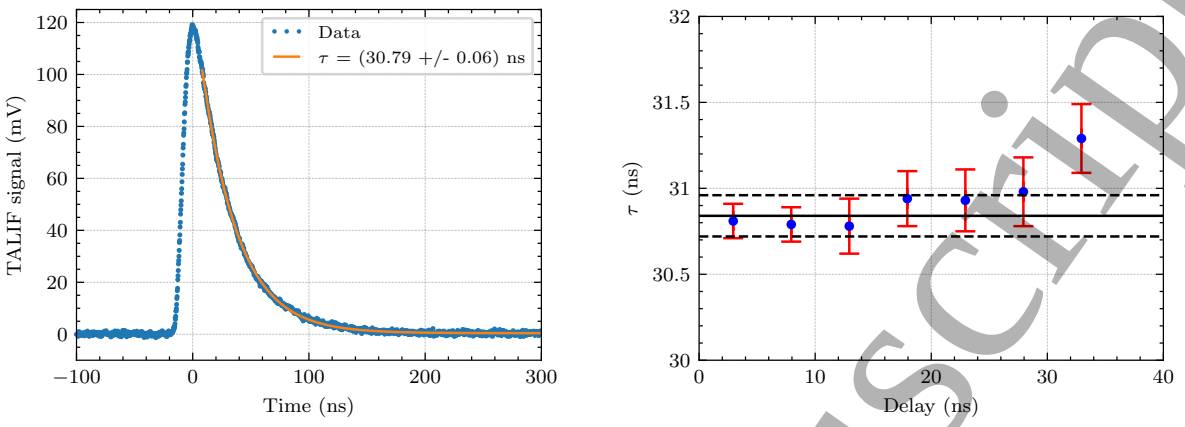

Figure 8. Left: instantaneous resonant TALIF signal recorded for a pressure of 19.1 Pa, with a photodissociation laser power of 1 W and a detection voltage $V_{\mathrm{PM}} = 0.7$ kV. Numerical fitting gives a decay time of 30.79 ± 0.06 ns. Right: Dependence of the decay time on the initial time of the exponential fitting. Eliminating the last, least significant point (at about 33 ns), averaging provides a mean value of $\tau \simeq 30.84$ ns with an uncertainty of $2\,\sigma_{\mathrm{stat}} = 0.1$ ns.

A first term, in the uncertainty budget of the lifetime measurement, comes from the dependence of the best-fitting rate on the time domain over which fitting is performed. The corresponding uncertainty is such that $2\sigma_{\mathrm{stat}} = 0.1$ ns in the example shown on figure 8. A second term in the uncertainty budget comes from slower fluctuations that produce a systematic variation of the mean value given by short term measurements, when these measurements are repeated on the long term. The statistics of these more systematic fluctuations contribute another $2\sigma_{\mathrm{syst}} = 0.4$ ns.

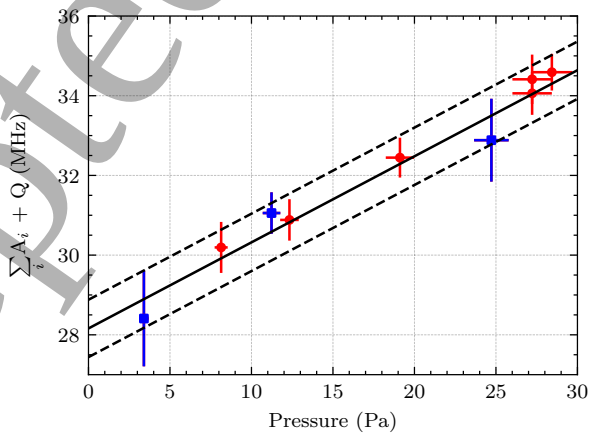

Figure 9. Stern–Volmer plot: de-excitation rate of the $(^3\mathrm{P}_2)6\mathrm{p}\,^2[1]^{\mathrm{o}}_{3/2}$ TALIF signal against the pressure. The measurement points are obtained with a plasma (blue square) or by photodissociation (red point). The uncertainty on the pressure is determined by the uncertainty on the temperature of the "cold finger", estimated at 0.5°C. The expanded uncertainty on the lifetime is the sum of the statistical and systematic uncertainties. We have not represented the uncertainty on the slope, which is ± 7 %.

Figure 9 shows a Stern-Volmer plot, i.e. the de-excitation rate of the TALIF signals as a function of pressure p, when atoms are produced either in a plasma or by photodissociation. The intercept at $p = 0$ determines the radiative lifetime ($\tau = 1/A$) of the $(^3\mathrm{P}_2)6\mathrm{p}\,^2[1]^\mathrm{o}_{3/2}$ states, as being 35.5 ± 0.9 ns. The linear variation of the de-excitation rate as a function of pressure gives the value of the quenching coefficient: $k = (9.0 \pm 1.3) \times 10^{-10}\,\mathrm{cm}^3\,\mathrm{s}^{-1}$.

The lifetime of the $(^3\mathrm{P}_2)6\mathrm{p}\,^2[1]^\mathrm{o}_{3/2}$ state has already been measured and calculated. Kono & Hattori (1979) measured a value of 39^{+4}_{-8} ns, with large possible systematic errors. Recently, new calculations of probabilities for some atomic iodine transitions yielded a τ value of 32.5 ± 1.2 ns (Filin et al. 2020). While coming closer to calculation than the former measurement, our result shows a slight discrepancy of theory with respect to experiment, which can open the way to more precise investigations.

5. Conclusion

The two-photon absorption laser induced fluorescence (TALIF) detection scheme has been applied to iodine. The excited levels $(^3\mathrm{P}_2)6\mathrm{p}\,^2[1]^\mathrm{o}_{3/2}$ and $(^3\mathrm{P}_2)6\mathrm{p}\,^2[3]^\mathrm{o}_{7/2}$ have been identified as possible targets for detection and monitoring of atomic iodine by two-photon absorption in the 300 nm region. Despite the fact atomic iodine is not as directly available in vapor form as xenon (which may have been the most widely observed atom by TALIF techniques), calibration of atomic iodine detection can be made robust, thanks to relative ease with which atomic iodine can be prepared in the laboratory, either by an electric discharge or by photodissociation. Direct two-photon excitation of upper states of I I, avoiding the intermediate $5p^5\,^2\mathrm{P}_{1/2}$ level the huge hyperfine structure of which may have spoiled the precision of ancient wavelength measurements, made it possible to measure the absolute energies of these states, through the use of an injection-seeded pulsed laser in a Doppler-free configuration. This atomic energy level re-calibration revealed that the tabulated excited spectrum of I I has displayed energies overestimated by $0.169(11)\,\mathrm{cm}^{-1}$ for several decades, which had only been suspected from a ground-level fine structure measurement in 1973.

As a matter of fact, the $\pm 0.005\,\mathrm{cm}^{-1}$ precision given by the NIST table of atomic energy levels was only the precision reached by Fourier-transform infrared spectroscopy in 1975, i.e. only the precision of the relative positions of the excited states, which was spuriously comprehended later as an uncertainty of the total excitation energies. In the present state of our knowledge and with the notable exception of the fine-structure components of the ground term, the hyperfine sublevels of which have been determined with a $\pm < 0.001\,\mathrm{cm}^{-1}$ precision, the precision on the energies of the excited levels of iodine does not appear to be possibly better than the precision achieved in the present work, generally $\pm 0.011\,\mathrm{cm}^{-1}$.

Temperature measurements based on the Doppler effect have also appeared quite feasible, even though they make it necessary to sort out what the TALIF profile owes to the hyperfine structure and what it owes to pure Doppler broadening. Relative

intensities of the hyperfine components have been found to obey the formula deduced from the expansion of the two-photon transition operator on irreducible tensors, which means that for any experiment where the iodine atom gets excited to final states of angular momentum $J_e \neq J_g = 3/2$, no additional variable parameter is needed. In case $J_e = J_g = 3/2$, the only additional parameter needed is the scalar-to-quadrupolar ratio of the two-photon transition, which can be either left as a single additional free parameter, or measured in a Doppler-free configuration, as we did for the $(^3P_2)6p\,^2[1]^o_{3/2}$ level. The lifetime of the $(^3P_2)6p\,^2[1]^o_{3/2}$ level was investigated as the limit of its de-excitation rate when the pressure tends to zero. The slight discrepancy between the obtained $\tau = 35.5(9)$ ns and the $\tau = 32.5(1.2)$ ns value obtained in an independent calculation can motivate further lifetime studies.

A touch of mystery remains with the detection of fine-structure excited iodine atoms, at the $5p^5\,^2P^o_{1/2}$ level, which was attempted through excitation of three different upper levels, but did not provide any evidence for the presence of $^2P^o_{1/2}$ atoms in the studied discharges. As excited iodine atoms have actually been detected starting from other molecules (Brewer et al. 1983, Tiee et al. 1983, Godwin et al. 1987, Tonokura et al. 1993), other detection schemes must be piloted in future experiments.

As an application of these basic measurements on atomic iodine, either in a photodissociation cell or in a plasma, atomic iodine ground state densities and gas temperatures are on the way to be measured in iodine-fed thrusters, i.e. in plasmas between 0.1 and 4 Pa (Esteves et al. 2022). That pressure range makes TALIF appear as a quite suitable technique for such diagnostics, as it has been shown in the present work to provide a detection scheme sensitive enough at pressures around 1 Pa.

Acknowledgments

The authors acknowledge financial support from the Agence innovation défense of the Délégation générale de l'armement (DGA), École Polytechnique and fédération de recherche Plas@par (contract No. FR2040). This work has also benefited from the Plasma Science and Training project managed by the Agence nationale de la recherche as part of national programme Investissements d'avenir (contract No. ANR-18-EURE-0014).

References

Ambalampitiya H B, Hamilton K R, Zatsarinny O, Bartschat K, Turner M A, Dzarasova A & Tennyson J 2021 *Atoms* **9**(4), 103.

Ashok C, Vishwakarma S, Bhatt H & Deo M 2019 *J. Quant. Spectrosc. Ra.* **235**, 162.

Bamford D J, Dyer M J & Bischel W K 1987 *Phys. Rev. A* **36**, 3497.

Biraben F, Cagnac B & Grynberg G 1974 *Phys. Rev. Lett.* **32**(12), 643.

Blondel C 2020 *Phys. Rev. A* **101**(1), 016501.

Booth J P, Marinov D, Foucher M, Guaitella O, Bresteau D, Cabaret L & Drag C 2015 *J. Instrum.* **10**(11), C11003.

Brewer G R, Currie M R & Knechtli R C 1961 *Proceedings of the IRE* **49**(12), 1789.

Brewer P, Das P, Ondrey G S & Bersohn R 1983 *J. Chem. Phys.* **79**(2), 720–723.
Brunet H, Chauvet P, Mabru M & Torchin L 1985 *Chem. Phys. Lett.* **117**(4), 371.
Cabaret L & Drag C 2010 *Eur. Phys. J.-Appl. Phys.* **51**(2).
Cerny D, Bacis R, Bussery B, Nota M & Vergès J 1991 *J. Chem. Phys.* **95**(8), 5790.
Chichinin A I 2006 *J. Phys. Chem. Ref. Data* **35**(2), 869–928.
Crosley D R & Bischel W K 1984 *Phys. Rev. A* **30**, 1546.
Cunge G, Ramos R, Vempaire D, Touzeau M, Neijbauer M & Sadeghi N 2009 *J. Vac. Sci. Technol. A: Vacuum, Surfaces and Films* **27**(3), 471.
Das P, Venkitachalam T & Bersohn R 1984 *J. Chem. Phys.* **80**(10), 4859.
Dietz P, Gärtner W, Koch Q, Köhler P E, Teng Y, Schreiner P R, Holste K & Klar P J 2019 *Plasma Sources Sci. Technol.* **28**(8), 084001.
Drag C, Marmuse F & Blondel C 2021 *Plasma Sources Sci. Technol.* **30**, 075026.
Engeln R, Klarenaar B & Guaitella O 2020 *Plasma Sources Sci. Technol.* **29**(6), 063001.
Engleman R, Keller R A & Palmer B A 1980 *Appl. Optics* **19**(16), 2767.
Eshbach F E & Fisher R A 1954 *J. Opt. Soc. Am.* **44**(11), 868–869.
Esteves B, Marmuse F, Drag C, Bourdon A, Alvarez Laguna A & Chabert P 2022 *Plasma Sources Sci. Technol.* **31**, 085007.
Filin D, Savukov I M & Colgan J 2020 *J. Phys. B: At. Mol. Opt. Phys.* **53**(14), 145003.
Flusberg A, Mossberg T & Hartmann S R 1976 *Phys. Rev. A* **14**, 2146.
Gazeli K, Lombardi G, Aubert X, Duluard C Y, Prasanna S & Hassouni K 2021 *Plasma* **4**(1), 145–171.
Godwin F, Gorry P, Hughes P, Raybone D, Watkinson T & Whitehead J 1987 *Chem. Phys. Lett.* **135**(1-2), 163.
Grondein P, Lafleur T, Chabert P & Aanesland A 2016 *Phys. Plasmas* **23**(3), 033514.
Grynberg G, Biraben F, Giacobino E & Cagnac B 1976 *Opt. Commun.* **18**.
Grynberg G, Biraben F, Giacobino E & Cagnac B 1977 *J. Phys. (Paris)* **38**, 629.
Grynberg G & Cagnac B 1977 *Rep. Prog. Phys.* **40**, 791.
Hunter T F & Leong C M 1987 *Chem. Phys.* **111**(1), 145–153.
Ip J & Burns G 1972 *J. Chem. Phys.* **56**(6), 3155–3161.
Jaccarino V, King J, Satten R & Stroke H 1954 *Phys. Rev.* **94**(6), 1798.
Katsoprinakis G, Chatzidrosos G, Kypriotakis J, Stratakis E & Rakitzis T 2016 *Sci. Rep.* **6**(1), 1–8.
Kiess C C & Corliss C H 1959 *J. Res. NBS A Phys. Chem.* **63**, 1.
Kono A & Hattori S 1979 *J. Opt. Soc. Am.* **69**(2), 253–255.
Kramida A E 2011 *Comp. Phys. Comm.* **182**(2), 419.
Kramida A, Yu. Ralchenko, Reader J & and NIST ASD Team 2021 NIST Atomic Spectra Database (ver. 5.9), [Online]. Available: `https://physics.nist.gov/asd` [2022, July 19]. National Institute of Standards and Technology, Gaithersburg, MD.
Kronfeldt H D & Loa I 1992 *Z. Phys. D* **24**, 211.
Larsen J J, Wendt-Larsen I & Stapelfeldt H 1999 *Phys. Rev. Lett.* **83**(6), 1123.
Lawrence G M 1967 *Astrophys. J.* **148**, 261.
Levko D & Raja L L 2021 *J. Appl. Phys.* **130**(17), 173302.
Liebl H & Harrison W W 1976 *Int. J. Mass. Spectrum* **22**(3-4), 237.
Lottigier P, Jucha A, Cabaret L, Blondel C & Drag C 2019 *Appl. Phys. B* **125**(1), 1–10.
Luc-Koenig E, Morillon C & Vergès J 1973 *Physica* **70**(1), 175–189.
Luc-Koenig E, Morillon C & Vergès J 1975 *Physica Scripta* **12**(4), 199.
Mazouffre S 2016 *Plasma Sources Sci. Technol.* **25**(3), 033002.
Minnhagen L 1962 *Ark. Fys.* **21**.
Mu X, Deng L, Huo X, Ye J, Windholz L & Wang H 2018 *J. Quant. Spectrosc. Ra.* **217**, 229.
Murakawa K 1938 *Z. Phys.* **109**(3), 162–174.
Murakawa K 1958 *J. Phys. Soc. Jap.* **13**(5), 484–492.
Murakawa K & Suwa S 1954 *Z. Phys.* **137**(5), 575–582.
Pindzola M S 1978 *Phys. Rev. A* **17**, 1021.

Rafalskyi D, Martínez J M, Habl L, Zorzoli Rossi E, Proynov P, Boré A, Baret T, Poyet A, Lafleur T, Dudin S et al. 2021 *Nature* **599**(7885), 411–415.

Saxon R P & Eichler J 1986 *Phys. Rev. A* **34**, 199.

Steinberger T E & Scime E E 2018 *Journal of Propulsion and Power* **34**(5), 1235–1239.

Stewart R S, Woolsey G A, Brown J M, Coulter J R M & Emeléus K G 1964 *in* 'Proceedings of the Royal Irish Academy. Section A: Mathematical and Physical Sciences' JSTOR pp. 85–91.

Tellinghuisen J 2011 *J. Chem. Phys.* **134**(8), 084301.

Tiee J J, Ferris M J, Loge G W & Wampler F B 1983 *Chem. Phys. Lett.* **96**(4), 422.

Tonokura K, Matsumi Y, Kawasaki M, Kim H L, Yabushita S, Fujimura S & Saito K 1993 *J. Chem. Phys.* **99**(5), 3461.

Wiesenfeld J R & Young R H 1981 *Chem. Phys.* **58**(1), 51.

Woolsey G A, Plumb I C & Lewis D B 1973 *J. Phys. D: Appl. Phys.* **6**(16), 1883.